The race of time during oxide-to-MOF conversion: Competition between MOF(Al) growth and alumina facets rearrangement

Limor Ben Neon, Mikhael Bechelany, Martin Drobek, Eddy Petit, Anne Julbe

The race of time during oxide-to-MOF conversion: Competition between MOF(Al) growth and alumina facets rearrangement

Limor Ben Neon[1], Mikhael Bechelany[1,2], Martin Drobek[1], Eddy Petit[1,3] and Anne Julbe[1]*

[1]Institut Européen des Membranes (IEM); Univ Montpellier, CNRS, ENSCM, Place Eugène Bataillon; 34095 Montpellier; France
[2]Gulf University for Science and Technology, GUST, Sabah Al-Salem; Kuwait
[3]UAR Plateforme d'Analyses et Caractérisations (PAC) Chimie Balard Montpellier, Univ Montpellier, CNRS, ENSCM, Place Eugène Bataillon; 34095 Montpellier; France

*corresponding author: anne.julbe@umontpellier.fr

Keywords: MOF-growth, facet rearrangement, microwave, morphology, competition, MOF-dissolution

Abstract

The direct growth of Metal-Organic-Frameworks (MOFs) on ceramic substrates is a promising strategy to promote their industrial implementation. Yet, the lack of deep scientific comprehension regarding the *in-situ* conversion of metal derivatives into MOFs, resulting in limited control over their crystal growth, morphology and distribution, hampers their up-scale production. In this work, we provide for the first time the experimental evidence that a competition between MOF formation and alumina facet rearrangement occurs at extended reaction times up to 90 minutes. We demonstrate that the facet rearrangement induced by pH variations dictates the final morphology and distribution of MOF(Al) crystals grown during the MW-assisted hydrothermal synthesis in water. Hence when facet-rich alumina substrate is used for oxide-to-MOF conversion, short reaction times ought to be applied.

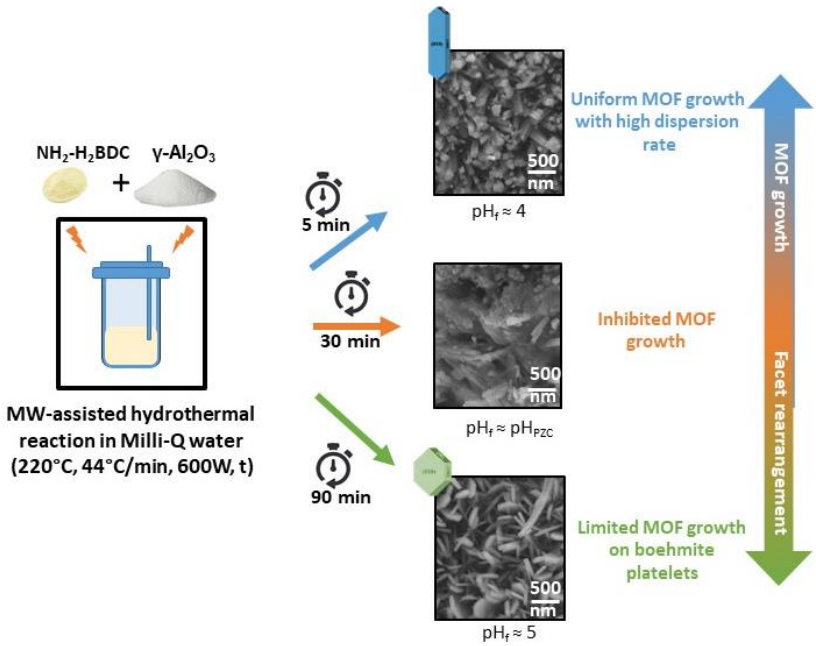

1. Introduction

Metal-organic-frameworks (MOF) are versatile materials endowed with a flexible porous structure. Their unique properties such as high porosity, stability, customizable morphology, as well as their breathing and gate-opening behavior, make them suitable for a wide-range of potential applications such as gas separation,[1] adsorption[2,3]or photo(electro)catalysis.[4][5] Notably, many MOFs can be easily obtained via a hydrothermal approach, though they are disadvantaged by long synthesis times. To overcome this drawback, several alternative synthesis procedures have been developed, including electrochemical, mechanochemical, sonochemical or MW-assisted synthesis routes.[6] An organic linker and a metal precursor are always required. Typically, two types of metal sources are employed: metal salts [3] or metal-derived substrates (e.g., oxide ceramics[7–9]; metals[10]). From an industrial perspective, the latter option, avoiding the use of metal salts, is more attractive as it permits the direct growth of MOFs on robust and mechanically stable supports such as membranes, films, foams, and pellets.[11] Moreover, this approach could aid in recycling industrial metal waste by using it as both the metal source and substrate, thereby promoting a circular economy.[12] On this basis, *in-situ* shaping of MOFs is often regarded as highly appealing, as it is environmentally friendly, simplifies large-scale handling of MOFs, and reduces health risks associated with powder manipulation.[11] Furthermore, several research works have shown that this synthesis approach promotes the epitaxial growth of well-organized MOF crystals, opening a new field of application in electronics and optics.[13,14] Despite the demonstrated advantages of converting metal-oxides to MOFs, many mechanistic aspects in terms of crystal growth and shape control are still unclear. As a result, maintaining effective control over these parameters on a large scale remains a significant challenge, limiting the feasibility of large-scale *in-situ* production of MOFs. Specifically, the aforementioned parameters are impacted by the chemical and physical conditions during reaction. For instance, it is well known that the formation of MOFs from metal salts is sensitive to parameters such as ligand concentration, solvent type, synthesis temperature/reaction time, pH and to the presence of additives/modulators.[15,16] In particular, the effects of the last two parameters are closely interlinked and often overlooked. In particular, the effects of the last two parameters are closely linked and often overlooked. Minor changes in pH can significantly affect MOF morphology, as already reported in other works.[16] Adding modulators during MOF synthesis improves control over both crystal shape and size. Modulators can be either surfactants acting as capping agents or monodentate additives.[16] They can affect the metal-linker coordination[17] and/or modulate the balance between deprotonated and protonated organic linkers in the synthesis solution.[18] By using monodentate additives as coordination modulators, the crystal growth of MOFs is better controlled due to the competitive interactions between the organic linker and the additive with metal ions.[16,17] Additionally, some additives can regulate the pH of the solution via acid-base reactions, making the pH of the additive an important factor to consider.[18] If the additive has an alkaline nature, the pH of the reaction solution increases, promoting the deprotonation of organic linkers. Subsequently, more organic linkers interact with metal ions, promoting the crystal nucleation kinetics and subsequently leading to the formation of small MOF crystals.

To the best of the authors' knowledge, the impact of pH on the direct growth of MOFs on ceramic substrates also serving as a metal source has never been considered until now. This is all the more important since the pH of the synthesis medium strongly influences the surface structure of metal oxides such as alumina-based compounds.[19–22]
As demonstrated in other works,[19–22] the pH of the medium can cause facet rearrangement on γ-alumina[20–22] and boehmite under hydrothermal conditions.[19] Hence, since their facets are

endowed with their own surface energy and hydrophilicity,[19,21] the directional growth of facet is pH-driven, favoring the formation of a specific morphology of alumina/ boehmite nanocrystals.[19–22] For example, at pH~4, bar-shaped crystals are favored while at higher pH values, a gradual transition occurs from hexagonal crystal to rhombic platelets.[19] According to several theoretical and computational studies, this change in facet distribution is caused by the difference in surface energy and hydrophilicity as well as the presence of soluble Al(III) tetrahedral sites on (110) alumina facets having a reactive nature in aqueous media.[19–22] In this context, it has been shown that even boehmite grown directly on aluminum in aqueous media adopts different shapes depending on the solution's pH.[22]
In this context, it remains uncertain whether the pH of the medium and the presence of acid-base modulators contribute to the surface reconstruction of alumina-based supports, which could in turn, influence the growth, size and morphology of the supported MOFs. Accordingly, these variations in the acido-basicity of the reaction medium could potentially affect surface properties and crystal distribution.

In this work, we provided for the first time experimental evidence that surface rearrangement and MOF growth compete with each other depending on the synthesis time. Indeed, via MW-assisted direct growth of MOF(Al) on γ-alumina particles, we observed a remodeling of both MOF and alumina crystals at prolonged reaction times caused by *(i)* the secondary reaction of decomposition and polymerization of the organic ligand 2-aminoterephthalic acid (NH_2-H_2BDC) under MW irradiation, and *(ii)* the pH variation occurring during the reaction. The latter was shown to have a strong impact on the surface reactivity of alumina and its facet rearrangement that dictates the final MOF morphology and crystal distribution.

1. Materials and methods

1.1. Synthesis

Alumina powder (γ-Al_2O_3) derived from boehmite was used as a substrate source of Al^{3+} for the growth of MOF(Al) crystals by MW-assisted conversion of the oxide. Boehmite (CATAPAL C1 alumina, Sasol) was calcined at 500°C for 3h in air in order to obtain γ-Al_2O_3 powder. Then, 1 g of this calcined boehmite (γ-Al_2O_3) was introduced into a Teflon liner containing 40 mL of a 1 wt% concentrated solution of 2-aminoterephthalic acid (NH_2-H_2BDC, Merck, 99%) in water (Milli-Q, 18MΩ). A Microsynth Milestone microwave oven equipped with an HPR 1000/10 rotor segments was used to heat the mixture at 220°C (44°C/min, 600W). Different MW irradiation times (t) at 600W were applied in order to study the impact of MOF(Al) crystal growth, dissolution and reconstruction of the alumina phase in function of time. The resulting samples are designated as t-BM, where t is the irradiation time (t = 5, 15, 30, 60 and 90 min) (Figure 1). After the MW-assisted conversion of Al_2O_3 to MOF(Al), samples were collected, washed with Milli-Q water/ DMF (N, N-Dimethylformamid, Sigma Aldrich, 99.8%)/ Milli-Q water, using a Sigma 3-16P centrifuge (8000 rpm, 5 min) and dried overnight at 120°C in an oven.

For comparison, as a reference sample, 1 g of calcined boehmite was heated at 220°C (600W; 44°C/min) for 90 min in Milli-Q water to observe the impact of neutral pH on the alumina surface. The sample is referred to as MilliQ-B. In addition, to evaluate the influence of facet rearrangement on MOF growth, we also utilized an amorphous alumina devoid of facets as a substrate for MOF(Al) conversion, as previously reported in our work elsewhere with minor modifications.[23] Briefly, in this case, SiC foams were coated with alumina by atomic layer deposition (ALD) and were converted under the same experimental conditions using NH_2-H_2BDC as an organic linker (cf. synthesis details in SI).

In all cases, the pH of the organic linker solution was measured before and after the reaction with pH indicator paper.

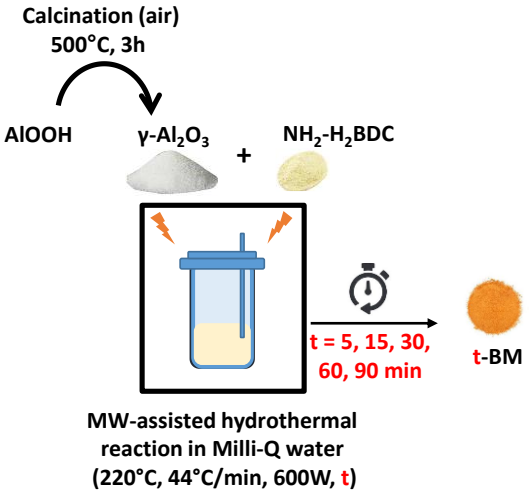

Figure 1: Schematic representation of the t-BM samples synthesis procedure.

1.2. Characterization

To ensure the reproducibility of the procedure and reinforce the made observations regarding the competition between MOF growth and alumina surface rearrangement, t-BM samples were synthetized three times. The surface morphology of these synthetized three batches as well as the elemental distribution of Al, O, N and C atoms were examined across five different sample zones using a Zeiss Sigma 300 SEM equipped with an Oxford Instruments X-Max ^{N} SDD detector for Energy Dispersive X-ray spectroscopy (EDX). Reported values in this study represent the mean values from these analyses across the three batches and five sample zones. Samples were metalized with platinum. To validate the formation of MOF(Al) and study its phase nature as well as the surface rearrangement of alumina facets that occurs, powder X-ray diffractograms (PXRD) were recorded with a Malvern Panalytical X'Pert Powder S using a scan rate of 0.021°/s. The precision in the diffraction peak position is 0.04° (2θ). Infra-red attenuated total reflectance (IR-ATR) spectra were taken using a Nicolet™ iS50 NEXUS FTIR spectrometer. In addition, X-ray photoelectron spectroscopy (XPS) analyses were carried out on 5-BM and 90-BM samples with an ESCALAB 250 (Thermo Electron) to characterize their surface chemistry. Al Kα (1486.6 eV) was used as a monochromatic excitation source. The analyzed surface area had a diameter of 500 µm. The spectra were calibrated according to the binding energy (BE) of the C-C bond (BE(C1s) = 284.8 eV). Peak fitting was performed with CasaXPS software using a Shirley type background. In order to understand the growth mechanism, synthesis solutions of 5-BM and 90-BM samples were analyzed using an Orbitrap ID-X spectrometer using ESI (Electro Spray Ionization) as an ionization source coupled with Vanquish LCMS and UHPLC systems (ThermoScientific) to determine the compounds formed from NH_2-H_2BDC in the absence of alumina substrate. In addition, these solutions were analyzed by carbon13 nuclear magnetic resonance spectroscopy (NMR^{13}C) to determine the presence of organic groups. Spectra were recorded at 298K using a UDEFT sequence (NS = 1024 scan) on a Bruker AVANCE III 500 NMR spectrometer equipped with a 5 mm Helium 1H/X BBO cryoprobe. Deuterated acetonitrile (CD_3CN, 99.96 at.% D, Sigma Aldrich) was used as a solvent. All data were processed with Bruker Topspin 3.6.2 software. The surface properties of the key samples- 5-BM, 30-BM and 90-BM- were analyzed using N_2 physisorption experiments. The samples were outgassed under vacuum at 150°C for 12h and N_2 adsorption/desorption isotherms were recorded using a Micromeritics ASAP 2020 instrument. The specific surface area (S_{BET}) was calculated using the multipoint Brunauer–Emmett–Teller (BET) method. The total pore volume (V_p) was determined at a

P/P_0 value close to 0.995. For comparison, N_2 physisorption was also performed on hydrothermally treated alumina (MilliQ-B).

2. Results

Surface morphology of MOF crystals grown on alumina particles (t-BM)

SEM images of the MOF(Al) crystals grown by conversion of γ-Al_2O_3 powder at different reaction times (samples referred to as t-BM with t = 5, 15, 30, 60, 90 min) are shown in Figure 2. We observe that the crystal morphology and distribution vary with MW irradiation time. Short synthesis times (~5 min) lead to small, thin and well-organized fibers homogeneously covering the surface of alumina particles. Meanwhile, longer reaction times up to 15 min resulted in a less homogeneous crystal size and shape distribution consisting of a mixture of fibrous and rectangular crystals. At 30 min, alumina particles are almost devoid of MOF crystals with a rare appearance of very small MOF(Al) crystals which could reflect either their complete dissolution or their initial growth state.

Surprisingly, after 60 min of reaction, crystals reappear in large quantity, but their shape differs from those observed at shorter reaction times. In fact, they rather exhibit a “bar-like” morphology with different sizes. Further extension of the reaction time (~ 90 min) leads to the formation of homogeneous and well-dispersed platelets. Their morphology is very similar to the boehmite (AlOOH) platelets obtained by Dohyeon Han *et al.*[22] after the hydrothermal treatment of AlOOH in water at neutral pH.

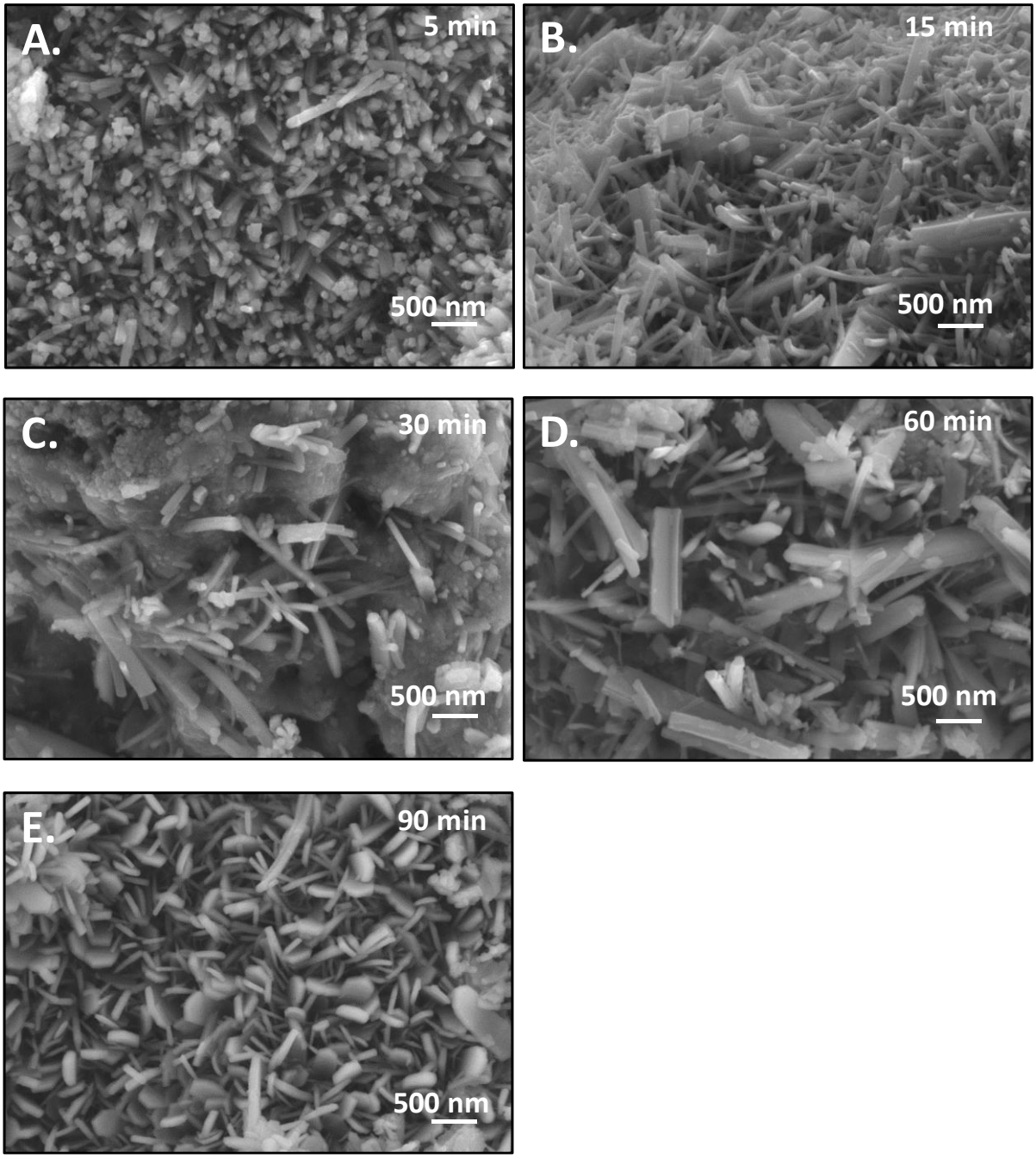

Figure 2: SEM images of t-BM samples obtained after MW-assisted hydrothermal conversion of γ-Al_2O_3 to MOF(Al), in the presence of NH_2-H_2BDC (600W, 44°C/min, 220°C), with increasing reaction times t: (A.) 5 min, (B.) 15 min, (C.) 30 min, (D.) 60 min, (E.) 90 min.

Similar results were also obtained in this work when subjecting γ-Al_2O_3 particles to MW irradiation solely in Milli-Q water (pH = 7) due to the rearrangement of alumina facets (Figure 3). It is therefore possible that during the conversion of alumina to MOF(Al) at prolonged reaction times, the MOF(Al) structure is altered by the effect of alumina surface restructuring which is strongly pH-dependent.[22] Indeed, we noticed considerable pH variations for each t-BM sample synthesis medium after reaction, as well as a color change of both the medium and the sample (Table 1, Table S2). Short reaction times induced an acidic pH medium (~ 4) whereas longer reaction times resulted in a relatively more neutral solution (pH ~ 5) (Table 1). Therefore, it is highly plausible that such pH variations affected the crystal

structure of alumina and MOF(Al), as suggested by the color evolution of both t-BM powder and their reaction medium from yellow to brown.

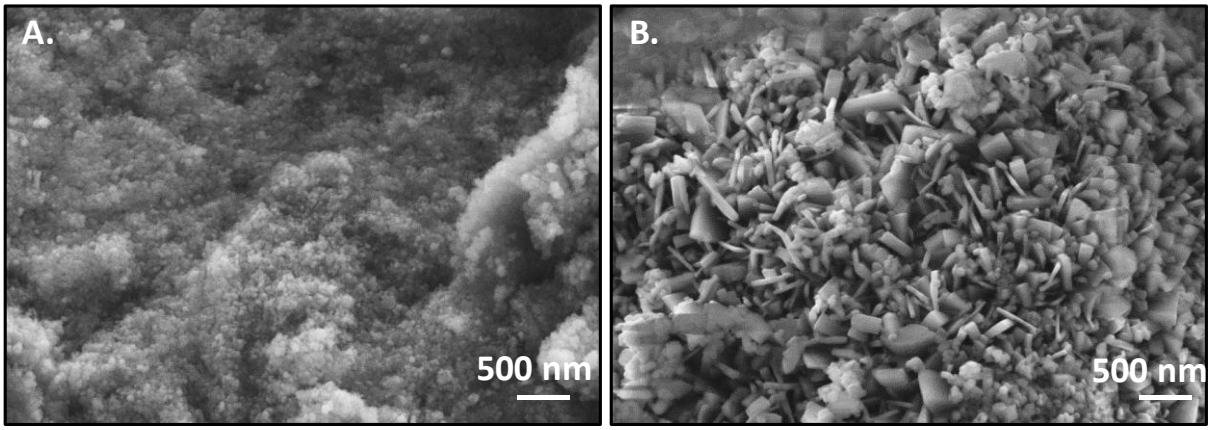

Figure 3: SEM images of (A) γ-Al_2O_3 obtained by calcination of boehmite at 500°C; (B) Platelets crystals grown on γ-Al_2O_3 after 90 min MW irradiation at 220°C (600W, 44°C/min) in water only.

Table 1: pH values measured before (pH_i) and after (pH_f) MW-assisted hydrothermal reaction of NH_2-H_2BDC in water with and without alumina substrate. The color of the samples after reaction is also reported.

Synthesis time (min)	**5**	**15**	**30**	**60**	**90**
t-BM sample color	Yellow	Yellow	Dark yellow	Brown	Dark brown
pH_i	6	6	6	6	6
pH_f (with alumina substrate)	4	4-5	5	5	5
pH_f (without alumina substrate)	3	3-4	4	4	4

Phase structure determination and chemical composition of t-BM samples

In order to evidence the impact of surface reconstruction on MOF(Al) crystal formation, XRD, IR-ATR, XPS and EDX analyses were applied to examine the surface of the samples. PXRD patterns clearly confirm the existence of a structural modification of γ-Al_2O_3 as well as the evolution of MOF(Al) phase as a function of synthesis time (Figure 4). After 5 min of reaction, the presence of a mixed phase comprising both γ-Al_2O_3 and boehmite was noted. The proportion of the latter increases with longer reaction times as revealed by the intensification of the diffraction peaks at 14.4°, 28.1°, 38.3°, 49.3°, 55.3°, 60.7° (Figure 4, Figure S1).[24,25] The maximum intensity was achieved for samples obtained after 90 min of reaction (90-BM). Meanwhile, a minor γ-Al_2O_3 phase was observed at 45.9°, 66.7°.[24] This phase evolution is also detected by IR-ATR spectroscopy. The characteristic absorption bands of boehmite hydroxide species are visible at 3296, 3090 and 1068 cm^{-1} (Figure 5, Figure S2).[26] Besides, the quantitative XPS analysis of 5-BM and 90-BM samples synthetized in 5 and 90 min respectively, highlights a drastic increase in the AlOOH/γ-Al_2O_3 ratio in the Al2p region which is multiplied by a factor of 3.7 (Table S4, Table S5). Simultaneously, we also noted a variation in the intensity and position of MOF(Al) diffraction peaks at 8.7°, 10.4°, 15.1°, 17.5°, 20.2°, 24.9° and 26.3° (Figure 4). Indeed, the intensity of the peaks decreases with increasing reaction times, indicating a decrease in the MOF concentration. Subsequently, for 90-BM, the peaks corresponding to MOF(Al) are barely visible reflecting a very low amount of MOF(Al). After 30 min of reaction, a new diffraction peak appears at 9.26° while maintaining a weak but stable intensity with longer reaction times. The synthesis time also has an impact on the position of the diffraction peaks. In particular, a slight shift of +0.16° and +0.20° for the peaks located at 8.7° and 17.5° was observed respectively (Figure 4B). These shifts could

indicate a change in the MOF lattice structure for extended reaction times. Moreover, it is worth noting that the obtained patterns do not correspond to either NH_2-MIL-53(Al) or MIL-53(Al) (Figure 4c). Hence, the expected formation of the NH_2-MIL-53(Al) phase did not occur.[27]

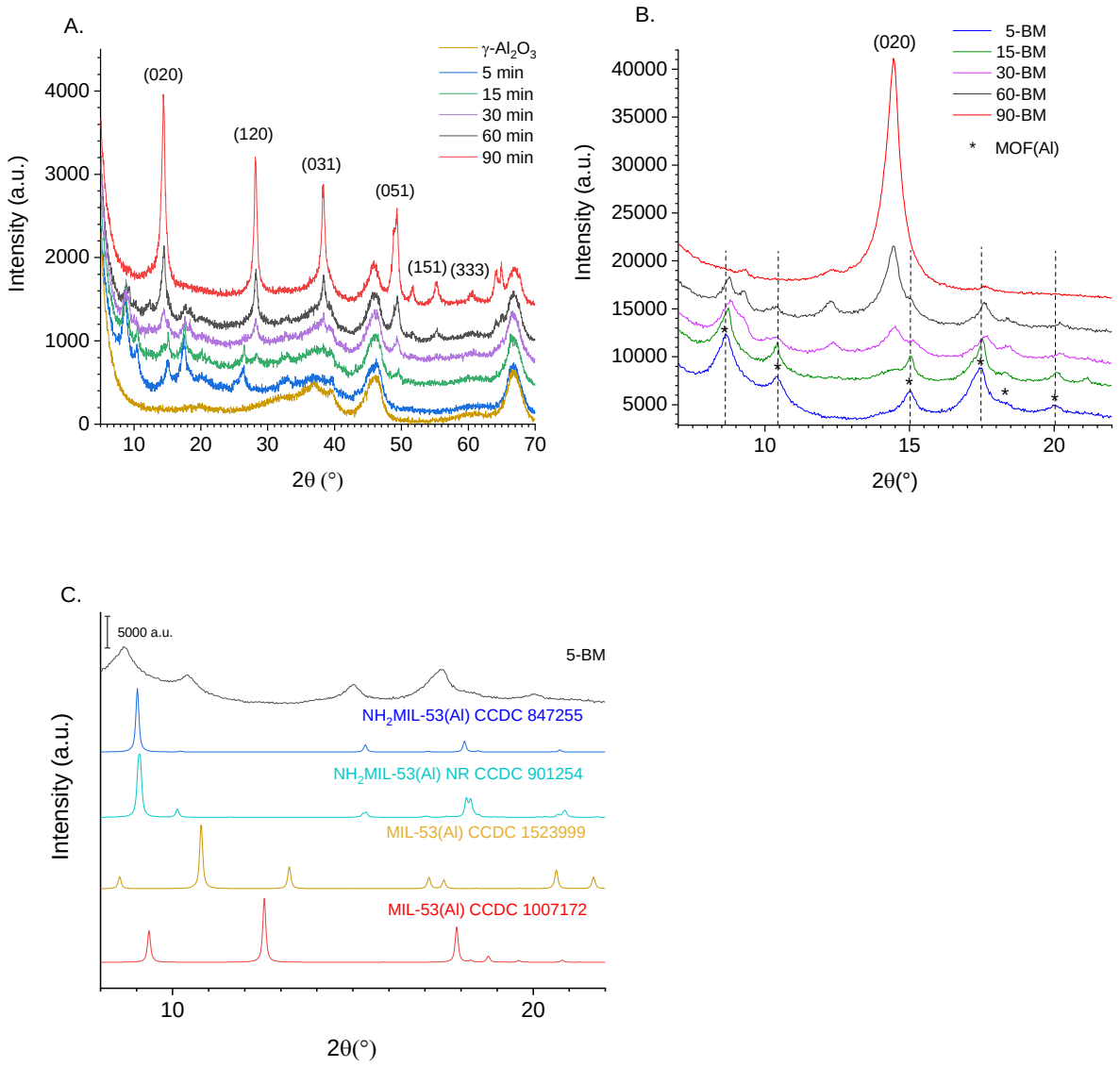

Figure 4: (A.) PXRD patterns of t-BM samples (t = 5, 15, 30, 60, 90 min) and the pristine γ-Al_2O_3 powder substrate. (B.) Zoom on the diffraction region of MOF(Al) for t-BM samples. (C.) Comparison of the simulated PXRD patterns for NH_2-MIL-53(Al) and MIL-53(Al) pure phases (CCDC), with the diffraction pattern of as-synthetized MOF(Al) phase for sample 5-BM.

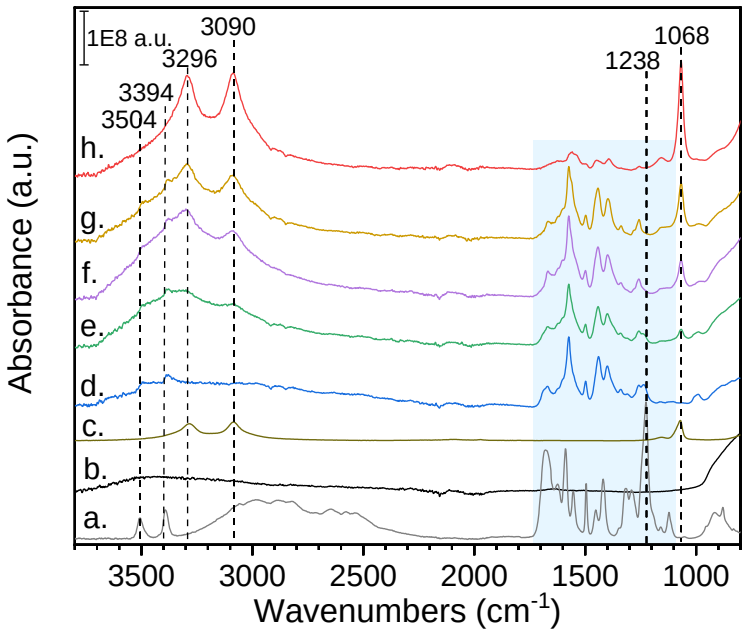

Figure 5: IR-ATR spectra of NH_2-H_2BDC (a.); γ-Al_2O_3 (b.); boehmite (c.), and t-BM samples (t = 5, 15, 30, 60, 90 min) (d-h respectively).

As shown in Figure 5, the characteristic IR absorption bands of the organic framework of t-BM samples observed between 1680 and 1225 cm^{-1} do not overlap with the absorption bands of the organic linker NH_2-H_2BDC. Thus, we can infer that the structure of the organic linker was modified indicating the formation of a different MOF(Al) type, which is in accordance with the PXRD results. Moreover, when NH_2-H_2BDC was hydrothermally treated in water and in the absence of alumina substrate under the same experimental conditions, the formation of different organic compounds such as $C_7H_8O_2N$, $C_{14}H_{13}O_3N_2$, $C_{10}H_{11}O_2$ or $C_8H_6O_3N$ was confirmed by ESI-FTMS analysis of the reaction medium after 5 and 90 min of reaction (Table S3). ^{13}C NMR analysis of the aforementioned solutions suggests the presence of ester and/or amide groups that are prone to form coordination complexes with Al^{3+} (Figure S7). These organic groups were also detected by XPS for 5-BM and 90-BM, also confirming the coordination of Al^{3+} with the carboxylate groups (Figure S9, Figure S10).
Hence, we conclude that during the MW-assisted conversion of alumina to MOF(Al), the initial organic linker (NH_2-H_2BDC) was immediately modified, resulting in the formation of a different framework via its coordination with Al^{3+}. Depending on the synthesis time, different nitrogen concentrations were measured for the as-prepared MOF(Al). Based on XPS measurements, the atomic percentage of amide groups is four times higher than the concentration of amine groups in 5-BM and this result is reversed for 90-BM (Table S4, Table S5). This result is consistent with the IR-ATR spectra of t-BM samples evidencing the gradual disappearance of $\nu(NH_2)$ at 3508 cm^{-1} and 3394 cm^{-1}. Thus, the chemical nature of MOF(Al) varies depending on the reaction time.

We also note that the reaction time influences MOF(Al) yields. Quantitative elemental analyses of t-BM samples carried out by EDX and XPS clearly show that at extended reaction times, the atomic concentration of C and N decreases (Figure 6, Table S4, Table S5). Indeed, comparing the chemical composition between 5-BM and 90-BM determined via XPS, a drop of 75 mol% of nitrogen and 73 mol% of carbon was observed. Given that both atoms are two fundamental elements of the organic structure, the obtained results emphasize a sharp decline in the direct growth of MOF(Al) on Al_2O_3 substrate. EDX mapping of 5-BM and 90-BM samples also highlights a change in the distribution of MOF(Al) crystals (Figure S3, Figure S4). While C, Al, O and N are uniformly distributed on the surface of 5-BM, carbon is barely observed on 90-BM.

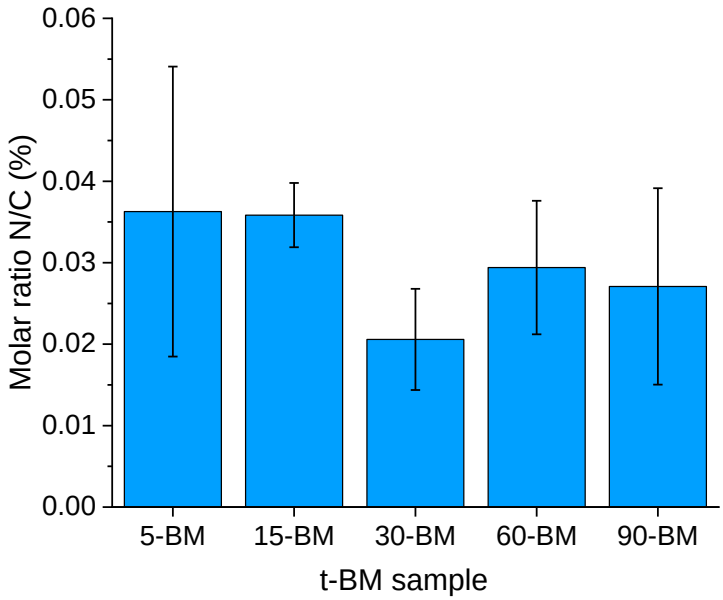

Figure 6: Evolution of the molar ratio between nitrogen and carbon (N/C, determined by EDX) for a series of t-BM samples prepared at different reaction times (t) (t = 5, 15, 30, 60 and 90 min).

Since the amount of formed MOF depends on the synthesis time and significantly affects the specific surface area of t-BM, noticeable variations in N_2 uptake were noticed. Textural analysis via N_2 sorption showed a clear trend in the specific surface areas of t-BM at reactions times of 5, 30 and 90 min (Table 2). Specifically, the BET surface area for 5-BM is the highest (226 m^2/g), but drops sharply to 47 m^2/g after 30 min of reaction. This value is comparable to the one of hydrothermally treated alumina in water (referred to as MilliQ-B. At longer reaction times (90 min), the specific surface area increases to 179 m^2/g for 90-BM.

Sample reference	S_{BET} (m^2/g)	V_p (cm^3/g)
MilliQ-B	44	0.228
90-BM	179	0.342
30-BM	47	0.120
5-BM	226	0.299
Catipol C1 Boehmite*	230	0.500

*Technical Data provided by Sasol (Sample outgassed at 300°C).

Table 2: Specific surface areas (S_{BET}) and pore volumes (V_p) determined by N_2 physisorption experiments for 5-BM, 30-BM and 90-BM, MilliQ-B and of Catipol C1 boehmite provided by Sasol.

3. Discussion

Formation of a crystalline MOF(Al) phase

Based on the PXRD analysis of t-BM samples, it can be concluded that the expected NH_2MIL-53(Al) phase was not formed. The structure of the MOF(Al) synthesized under MW irradiation does not match any of

the structures reported in the literature. The MW-assisted conversion of Al_2O_3 to MOF(Al) in the presence of NH_2-H_2BDC promotes the decarboxylation and amidation of the organic linker. The derived organic species are detected by ESI-FTMS and NMR^{13}C analysis (Figure S6, Figure S7) suggesting the presence of ester and amide groups that could coordinate with Al^{3+} and lead to the formation of a new metal-organic framework containing Al, C, O and N. The synthetized materials exhibit varying specific surface areas and pore volumes depending on reaction time. After 5 min and 90 min, high specific surface areas of approximately 226 m²/g and 179 m²/g are achieved, respectively, indicating the presence of highly porous structures. As a result, 5-BM and 90-BM could serve as promising materials for fluid purification and gas detection. Since the synthesis involves the direct growth of MOFs on alumina particles, isolating a single crystal to determine the lattice structure of the newly synthesized MOF phase is not feasible. A dedicated study would be required to fully characterize this MOF phase, which is beyond the scope of this work. Yet, the lack of crystallographic information does not undermine the observations regarding MOF crystal morphology, distribution, or the rearrangement of alumina facets during oxide-to-MOF conversion. Both phenomena appear to be correlated since they strongly depend on pH variation.

Impact of pH on alumina facets rearrangement

In the research work of D. Salionov *et al.*, it was shown that the formation of unsupported MIL-53(Al) involves three main steps: ligand deprotonation, nucleation and crystallization until pH stabilization.[28] Considering this reaction mechanism, the first step during *in-situ* formation of MOF on γ-Al_2O_3 in water corresponds to the deprotonation of NH_2-H_2BDC. This deprotonation can occur via an acid-base reaction with water and with alumina Bronsted and/or Lewis acid sites. This assumption seems to be validated by the observed decrease in pH from 6 to 4 in the presence of substrate and from 6 to 3 in its absence (Table 1). With increasing reaction time, the pH increases again and stabilizes at pH ~ 5 after 15 min in the presence of alumina substrate. The same pH evolution is observed in the absence of alumina when NH_2-H_2BDC is hydrothermally treated in water under MW irradiation. Therefore, it can be stated that the ligand is completely deprotonated after 30 min of reaction. Since different pH values are reached at different reaction times, the amount of hydrolyzed oxygen sites on γ-Al_2O_3 is expected to vary.[29] Indeed, Di Liberto *et al.* demonstrated via DFT calculations that specific oxygen sites located on the (001) γ-Al_2O_3 facets are sensitive to pH variation due to their difference in acidity.[29] These sites are responsible for water dissociation and exhibit two pKa values (pKa1 = 4.29; pKa2 = 9.06). At 4.29, an equilibrium between hydrolyzed oxygen sites (OsH^+) on the (001) facets and the free oxygen sites (Os) is established. Based on the pH measured for the reaction medium of 5-BM, the equilibrium zone favoring the direct formation of MOF crystals on γ-Al_2O_3 is reached. Simultaneously, hydration of the tetrahedral Al sites also occurs on the hydrophilic (110) facet at any pH value.[21] Subsequently, based on the DFT calculation of Reocreux *et al.,*[30] water favors the formation of AlO_xH_y species (boehmite) on the γ-Al_2O_3 surface. This transformation is visible on PXRD patterns as well as on XPS and IR spectra when reaction times are longer than 5 min, leading to the solubilization of Al^{3+} via Al-O-Al cleavage (Figure 4, Figure 5, Figure S8). Consequently, the perpetual release of Al^{3+} allows the formation of the MOF(Al).

Impact of pH variation during reaction on the dispersion and morphology of MOF(Al) crystals

It has been shown that the crystallization of the nuclei starts when a maximum concentration of deprotonated linker is reached and stops once the pH stabilizes, indicating the complete deprotonation of all ligand molecules.[28] After 15 min of reaction, the pH stabilizes around 5 (Table 1). Similarly, the acid-base reaction between water and the derived NH_2-H_2BDC compounds also stops within this time interval. It can be deduced that between 15 and 30 min of MW-assisted synthesis, the crystallization of MOF(Al) was completed due to the absence of protonated NH_2-H_2BDC derivatives. Subsequently, the competition between crystal growth and dissolution is driven by the dissolution of MOF(Al) crystals. This assumption explains the nearly bare surface of γ-Al_2O_3 evidenced by SEM-EDX analysis for 30-BM in which

the lowest amount of nitrogen and carbon (constituting elements of MOF) was detected. Additionally, the specific surface area obtained for 30-BM matches closely to the one of hydrothermally treated boehmite in water for 90 min under MW irradiation. This suggests that the amount of supported MOF on the alumina is minimal and does not significantly affect the specific surface area. At this stage, it appears that MOF growth is hindered. This hampering may be due to the near-neutral pH of the reaction medium after 30 min, which coincides with the point-of-zero charge (pH_{PZC}) of alumina.[29] At this pH, an equal number of positively and negatively charged species (H^+ and OH^-) are adsorbed on the alumina surface. In other words, a water layer surrounds the alumina surface, presumably preventing the adsorption of organic linkers and/or adducts on the surface, since the required anchoring sites are not accessible. This would explain the low amount of carbon and nitrogen measured on 90-BM by EDX (Figure S4) and XPS (Table S5). Subsequently, due to the hindered adsorption of organic linkers, the rearrangement of the surface structure is favored leading to the formation of hexagonal boehmite platelets observed by SEM and detected by PXRD, XPS and IR-ATR analysis. Indeed, the intensity of boehmite diffraction peaks intensifies for 30-, 60- and 90-BM samples while those of MOF(Al) are barely detected (Figure 4). Similar boehmite platelet crystals were observed when γ-Al_2O_3 was hydrothermally treated under the same experimental conditions only in the presence of water (i.e., at neutral pH), which is consistent with other reports in the literature.[19,22,25] Indeed, the studies by Rosso et al. [19] and Lee et al. [22] show that alumina facets respond sensitively to pH changes, leading to the hydroxylation of surface alumina into boehmite and subsequent facet rearrangement. This process induces the formation of distinct boehmite nanocrystals due to (i) variations in surface energies across AlOOH facets and (ii) the reactive nature of tetrahedral Al-sites. As pH increases, the (001) facet of alumina is shrinking while the (100) facet expands, ultimately forming platelets.

However, although the pH of the medium is stabilized after 30 min of reaction, it remains difficult to explain the different shapes of boehmite crystals obtained after 60 and 90 min of reaction (60-BM and 90-BM samples). SEM images (Figure 2D, E) show the presence of elongated bars for 60-BM while homogenous and well-organized platelets are observed for 90-BM.

The difference in crystal morphology and their homogeneity could be induced by a pH gradient occurring at the surface of the alumina substrate. It is plausible that MW irradiation (well known to enhance reaction kinetics and decrease activation energies)[31] overcomes the energy barrier required for organic linker molecules to pass through the water layer and interact with boehmite nanocrystals that have grown via facet rearrangement on the alumina substrate. The pH gradient induced at the surface decreases when reaction time increases due to pH stabilization. Subsequently, uniform platelets are formed after 90 min of reaction.

Considering these observations, it can be assumed that the rearrangement of the boehmite facets imposes the final morphology of the MOF(Al) crystals at long reaction times but limits their distribution on its surface due to the small difference between the pH_{PZC} of boehmite and the pH of the reaction medium. This explains the significant difference in specific surface area (∼74%) between the supported MOF samples after 30 and 90 min of reaction. The simultaneous formation of a small amount of MOF, along with the hydroxylation of the alumina surface into AlOOH, contributes to the increase of porosity.

Validation of the effect of alumina facet rearrangement on the morphology of MOF(Al) crystals

A simple way to test our assumption about the influence of facet rearrangement on MOF(Al) morphology is to use an alumina substrate having no distinct crystalline facets, such as amorphous alumina. Indeed in our previous work we demonstrated the possibility of converting ALD-alumina deposited on ceramic foams into MOF(Al) via a MW-assisted hydrothermal reaction under the same experimental conditions.[23] Hence, for comparison purposes, we replicated the reported synthesis procedure using

NH_2-H_2BDC as organic linker and we analyzed the products obtained after 30 and 90 min. Based on SEM-EDX analysis, the morphology of the ALD-alumina-derived MOF(Al) crystals remained unchanged after 30 and 90 min of reaction (Figure 7) with a homogeneous distribution (Figure S5). It is obvious that the morphology of the ALD-alumina-derived MOF crystals is completely different from the morphology obtained for the t-BM samples, although the pH of their reaction media is similar. This finding thus supports the conclusion that for crystalline alumina *(i)* the facet rearrangement is in direct competition with the MOF growth and *(ii)* the pH-dependent shape of their facets directs the final MOF(Al) crystal shape.

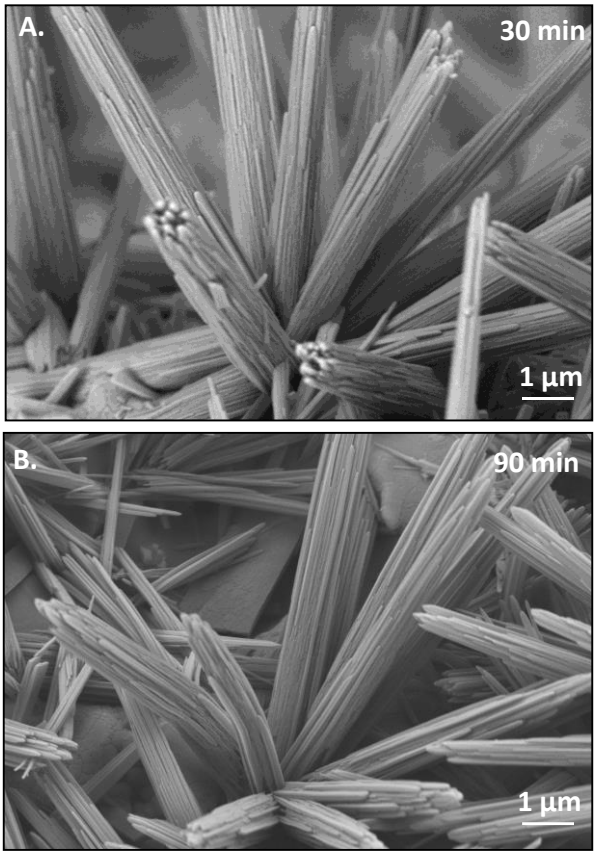

Figure 7: FESEM images of MOF(Al) crystals grown on SiC foams by hydrothermal conversion of ALD-alumina in the presence of NH_2-H_2BDC under MW-irradiation (MW power: 600W) at 220°C for 30 min (A.) and 90 min (B.).

4. Conclusion

This work provides the first experimental evidence that the *in-situ* conversion of alumina to MOF is influenced by the rearrangement of alumina facets. Indeed, depending on the pH of the synthesis medium, the surface morphology of alumina changes due to surface hydroxylation. We demonstrated that with increasing synthesis time under MW irradiation, the rearrangement of alumina facets dictates the final morphological structure of MOF(Al) crystals. To support this finding a compelling evidence was provided by comparing the morphology of MOF(Al) crystals grown on two different alumina substrates. MOF(Al) crystals generated from amorphous ALD-alumina coating maintained their morphology independent of the reaction time. The opposite was observed for MOF(Al) grown directly on γ-Al_2O_3 particles with crystal facets. Reaction times exceeding 15 min resulted in a decrease in MOF distribution while the MOF(Al) crystal morphology was dictated by the pH-dependent rearrangement of the γ-Al_2O_3 facets. We hypothesize that the formation of a water layer on the

alumina substrate, caused by the similar pH values between the reaction medium and the pH at the point of zero charge (pH_{PZC}) of alumina at 30 min, prevents the direct growth of MOF(Al).
Hence, in order to achieve maximum conversion of alumina-to-MOF, short MW-assisted reaction times are preferred (i.e., ~5 min). Another option to avoid facet rearrangement and promote MOF(Al) crystal growth is to favor facet-free substrates such as ALD-alumina.
With this work, we hope to raise the awareness of alumina facet rearrangement and its key role in the alumina-to-MOF conversion. Moreover, this phenomenon might also be observed for other oxides materials with pH-dependent facets, such as ZnO, TiO_2 or MgO, which will be explored in our upcoming publication. The potential to convert these oxides into MOFs, either through a MW-assisted method [32] or other techniques [33,34], has already been demonstrated in the literature. A theoretical computational study will also be conducted in future work to better understand the underlying mechanisms and optimize the conversion of selected metal oxides into MOFs.

Author Contributions

Conceptualization, L.B.N. and A.J.; methodology, L.B.N. and A.J.; validation, A.J.;
Investigation, L.B.N., E.P.; data curation, L.B.N.;
Writing—original draft preparation, L.B.N.; Review and editing, L.B.N., M.D., M.B., and A.J.;
Supervision, project administration and funding acquisition, A.J.

All authors have read and agreed on the published version of the manuscript. The authors declare that they have no known competing financial interests or personal relationships that could have appeared to influence the work reported in this paper.

Acknowledgments

This research was funded by the French National Research Agency (ANR project PEHY-0016-BHyoLOHC). The authors thank Bertrand Rebiere (UAR Plateforme d'Analyses et Caractérisations (PAC) Chimie Balard Montpellier, Univ Montpellier, CNRS, ENSCM) for SEM-EDX analyses.

Additional information

Supplementary material is supplied with this manuscript.

Data availability

Additional data will be made available on request.

References

[1] Lin R, Xiang S, Zhou W, Chen B. Microporous Metal-Organic Framework Materials for Gas Separation. Chem 2020;6:337–63. https://doi.org/10.1016/j.chempr.2019.10.012.

[2] Liu H, Fu T, Mao Y. Metal − Organic Framework-Based Materials for Adsorption and Detection of Uranium (VI) from Aqueous Solution. ACS Omega 2022;7:14430–56. https://doi.org/10.1021/acsomega.2c00597.

[3] Tran T Van, Jalil AA, Thi D, Nguyen C, Alhassan M, Nabgan W, et al. A critical review on the synthesis of NH2 -MIL-53 (Al) based materials for detection and removal of hazardous pollutants. Environ Res 2023;216:114422. https://doi.org/10.1016/j.envres.2022.114422.

[4] Rehman TU, Agnello S, Gelardi FM, Lazzara G, Buscarino G, Cannas M, et al. Unveiling the MIL-53 (Al) MOF : Tuning Photoluminescence and Structural Properties via Volatile Organic Compounds Interactions. Nanomaterials 2024;14.

[5] Sun Q, Chen D, Huang Q, Huang S, Qian J. Carbon nanotubes anchored onto hollow carbon for efficient oxygen reduction. Sci China Mater 2023;66:641–50. https://doi.org/10.1007/s40843-022-2173-3.

[6] Topologies MOF, Stock N, Biswas S. Synthesis of Metal-Organic Frameworks (MOFs): Routes to Various MOF Topologies, Morphologies, and Composites. Chem Rev 2012:933–69.

[7] Drobek M, Bechelany M, Vallicari C, Abou Chaaya A, Charmette C, Salvador-Levehang C, et al. An innovative approach for the preparation of confined ZIF-8 membranes by conversion of ZnO ALD layers. J Memb Sci 2015;475:39–46. https://doi.org/10.1016/j.memsci.2014.10.011.

[8] Drobek M, Kim JH, Bechelany M, Vallicari C, Julbe A, Kim SS. MOF-Based Membrane Encapsulated ZnO Nanowires for Enhanced Gas Sensor Selectivity. ACS Appl Mater Interfaces 2016;8:8323–8. https://doi.org/10.1021/acsami.5b12062.

[9] Ruan H, Guo C, Yu H, Shen J, Gao C, Sotto A, et al. Fabrication of a mil-53(al) nanocomposite membrane and potential application in desalination of dye solutions. Ind Eng Chem Res 2016;55:12099–110. https://doi.org/10.1021/acs.iecr.6b03201.

[10] Ji H, Hwang S, Kim K, Kim C, Jeong NC. Direct in Situ Conversion of Metals into Metal-Organic Frameworks: A Strategy for the Rapid Growth of MOF Films on Metal Substrates. ACS Appl Mater Interfaces 2016;8:32414–20. https://doi.org/10.1021/acsami.6b12755.

[11] Ma Q, Zhang T, Wang B. Shaping of metal-organic frameworks, a critical step toward industrial applications. Matter 2022;5:1070–91. https://doi.org/10.1016/j.matt.2022.02.014.

[12] Boukayouht K, Bazzi L, Hankari S El. Sustainable synthesis of metal-organic frameworks and their derived materials from organic and inorganic wastes. Coord Chem Rev 2023;478:214986. https://doi.org/10.1016/j.ccr.2022.214986.

[13] Gu Z, Zhang J. Epitaxial growth and applications of oriented metal – organic framework thin films. Coord Chem Rev 2019;378:513–32. https://doi.org/10.1016/j.ccr.2017.09.028.

[14] Linares-Moreau M, Brandner LA, Velásquez-Hernández M de J, Fonseca J, Benseghir Y, Chin JM, et al. Fabrication of Oriented Polycrystalline MOF Superstructures. Adv Mater 2024;36.

[15] Cheng X, Zhang A, Hou K, Liu M, Wang Y, Song C, et al. Size- and morphology-controlled NH2-MIL-53(Al) prepared in DMF-water mixed solvents. Dalt Trans 2013;42:13698–705. https://doi.org/10.1039/c3dt51322j.

[16] Łuczak J, Kroczewska M, Baluk M, Sowik J, Mazierski P, Zaleska-Medynska A. Morphology control through the synthesis of metal-organic frameworks. Adv Colloid Interface Sci 2023;314. https://doi.org/10.1016/j.cis.2023.102864.

[17] Hailing Guo , Yongzhong Zhu , Shilun Qiu , Johannes A. Lercher HZ. Coordination Modulation Induced Synthesis of Nanoscale Eu1-xTbx-Metal-Organic Frameworks. Adv Mater 2010:4190–2.

[18] Guo H, Zhu Y, Wang S, Su S, Zhou L, Zhang H. Combining coordination modulation with acid-base adjustment for the control over size of metal-organic frameworks. Chem Mater 2012;24:444–50. https://doi.org/10.1021/cm202593h.

[19] Zhang X, Cui W, Page KL, Pearce CI, Bowden ME, Graham TR, et al. Size and Morphology Controlled Synthesis of Boehmite Nanoplates and Crystal Growth Mechanisms. Cryst Growth Des 2018;18:3596–606. https://doi.org/10.1021/acs.cgd.8b00394.

[20] Pigeon T, Chizallet C, Raybaud P. Revisiting γ-alumina surface models through the topotactic transformation of boehmite surfaces. J Catal 2022;405:140–51.

https://doi.org/10.1016/j.jcat.2021.11.011.

[21] Réocreux R, Girel, Clabaut P, Tuel A, Besson M, Chaumonnot A, et al. Reactivity of shape-controlled crystals and metadynamics simulations locate the weak spots of alumina in water. Nat Commun 2019;10:1–8. https://doi.org/10.1038/s41467-019-10981-9.

[22] Han D, Lee D. Morphology controlled synthesis of γ-Al2O3 nano-crystallites in Al@Al2O3 core-shell micro-architectures by interfacial hydrothermal reactions of al metal substrates. Nanomaterials 2021;11:1–13. https://doi.org/10.3390/nano11020310.

[23] Ben Neon L, Drobek M, Bechelany M, Rebiere B, Julbe A. Microwaves induced epitaxial growth of urchin like MIL - 53 (Al) crystals on ceramic supports. Sci Rep 2024;53:1–8. https://doi.org/10.1038/s41598-024-71150-7.

[24] Stuart NM, Sohlberg K. The microstructure of γ-alumina. Energies 2021;14:1–16. https://doi.org/10.3390/en14206472.

[25] Lee J, Jang EJ, Jeong HY, Kwak JH. Critical role of (100) facets on γ-Al2O3 for ethanol dehydration: Combined efforts of morphology-controlled synthesis and TEM study. Appl Catal A Gen 2018;556:121–8. https://doi.org/10.1016/j.apcata.2018.02.018.

[26] Ludwig B. Infrared Spectroscopy Studies of Aluminum Oxide and Metallic Aluminum Powders, Part II: Adsorption Reactions of Organofunctional Silanes. Powders 2022;1:75–87. https://doi.org/10.3390/powders1020007.

[27] Bolinois L, Kundu T, Wang X, Wang Y, Hu Z, Koh K, et al. Breathing-induced new phase transition in an MIL-53(Al)-NH2 metal-organic framework under high methane pressures. Chem Commun 2017;53:8118–21. https://doi.org/10.1039/c7cc02743e.

[28] Salionov D, Semivrazhskaya OO, Casati NPM, Ranocchiari M, Bjelić S, Verel R, et al. Unraveling the molecular mechanism of MIL-53(Al) crystallization. Nat Commun 2022;13:1–9. https://doi.org/10.1038/s41467-022-31294-4.

[29] Liberto G Di, Maleki F, Pacchioni G. pH Dependence of MgO, TiO2, and γ-Al2O3 Surface Chemistry from First Principles. J Phys Chem C 2022:10216–23.

[30] Réocreux R, Girel E, Clabaut P, Tuel A, Besson M, Chaumonnot A, et al. Reactivity of shape-controlled crystals and metadynamics simulations locate the weak spots of alumina in water HAL Id : hal-02275963 Reactivity of shape-controlled crystals and metadynamics simulations locate the weak spots of alumina in water. Nat Commun 2019. https://doi.org/10.1038/s41467-019-10981-9.

[31] Ji T, Yang Z, Song S, Zhou T, Mu L, Lu X, et al. Intense microwave heating at strongly polarized solid acid/water interface for energy-efficient platform chemical production. Chem Eng Sci 2022;262:118035. https://doi.org/10.1016/j.ces.2022.118035.

[32] Bechelany M, Drobek M, Vallicari C, Abou Chaaya A, Julbe A, Miele P. Highly crystalline MOF-based materials grown on electrospun nanofibers. Nanoscale 2015;7:5794–802. https://doi.org/10.1039/c4nr06640e.

[33] Khan MA, Safira AR, Aadil M, Kaseem M. Development of anti-corrosive coating on AZ31 Mg alloy modified by MOF / LDH / PEO hybrids. J Magnes Alloy 2024;12:586–607. https://doi.org/10.1016/j.jma.2023.12.004.

[34] Chai L, Zhang L, Wang X, Xu L, Han C, Li T, et al. Bottom-up synthesis of MOF-derived hollow N-doped carbon materials for enhanced ORR performance. Carbon N Y 2019;146:248–56. https://doi.org/10.1016/j.carbon.2019.02.006.

Supplementary information

The race of time during oxide-to-MOF conversion: Competition between MOF(Al) growth and alumina facets rearrangement

Limor Ben Neon[1], Mikhael Bechelany[1,2], Martin Drobek[1], Eddy Petit[1,3] and Anne Julbe[1]*

[1]Institut Européen des Membranes (IEM); Univ Montpellier, CNRS, ENSCM, Place Eugène Bataillon; 34095 Montpellier; France
[2]Gulf University for Science and Technology, GUST, Sabah Al-Salem; Kuwait
[3]UAR Plateforme d'Analyses et Caractérisations (PAC) Chimie Balard Montpellier, Univ Montpellier, CNRS, ENSCM, Place Eugène Bataillon; 34095 Montpellier; France

*corresponding author: anne.julbe@umontpellier.fr

Direct growth of MOF(Al) on alumina-coated SiC via ALD:

- **Conditioning of ceramic foams**

Ceramic foams composed of SiC with 10 ppi (pores per inch) were supplied by EPMF-France (SEDEX-SiC-10 PPI). Before use, they were cut into pieces of 0.5 x 1.5 x 1.5 cm and then washed thoroughly with tap water, Milli-Q water and finally with ethanol (≥ 99.8%, Sigma Aldrich). After drying at 120°C overnight, the foams were thermally treated in air at 500°C for 4h (5°C/min).

- **Atomic Layer Deposition (ALD) of Al_2O_3**

The as-conditioned SiC foams were coated with Al_2O_3 by ALD using trimethyaluminum (TMA, Sigma Aldrich 97%, 25 sccm) and H_2O as precursors (25 sccm). Argon (≥ 99.999%, Linde Electronics) was used as sweep gas (100 sccm) and carrier gas (25 sccm). 250 cycles were carried out to obtain an average coating thickness of 50 nm. For each cycle, the TMA pulse, exposure, and purge times were 0.4 s, 30 s and 40 s, respectively. For H_2O, they were 2 s, 30 s and 40 s, respectively. Prior to deposition, the reactor chamber was maintained at 100°C under vacuum ($3x10^{-2}$ mbar).

- **Oxide-to-MOF conversion**

The thin layer of ALD-Al_2O_3 on SiC foams was converted to N-doped MOF(Al) using a MW-assisted hydrothermal synthesis protocol. Briefly, 0.4 g of 2-aminoterephthalic acid (NH2-H2BDC) (99%, Merck) was dissolved in 40 mL of Milli-Q water (1 wt% NH2-H2BDC solution). This reaction solution and the alumina-coated foams were transferred to a Teflon™ pressure vessel and heated for 1.5h at 220°C under microwave irradiation (MW power: 600W, 44°C/min) using a Milestone Microsynth microwave oven equipped with an HPR 1000/10 rotor. After the reaction, the MOF-decorated ceramic foams were recovered from the Teflon vessel and washed first with Milli-Q water, then with DMF and finally with Milli-Q water again to remove the DMF. Eventually, the samples were dried at 120°C for 12h in air.

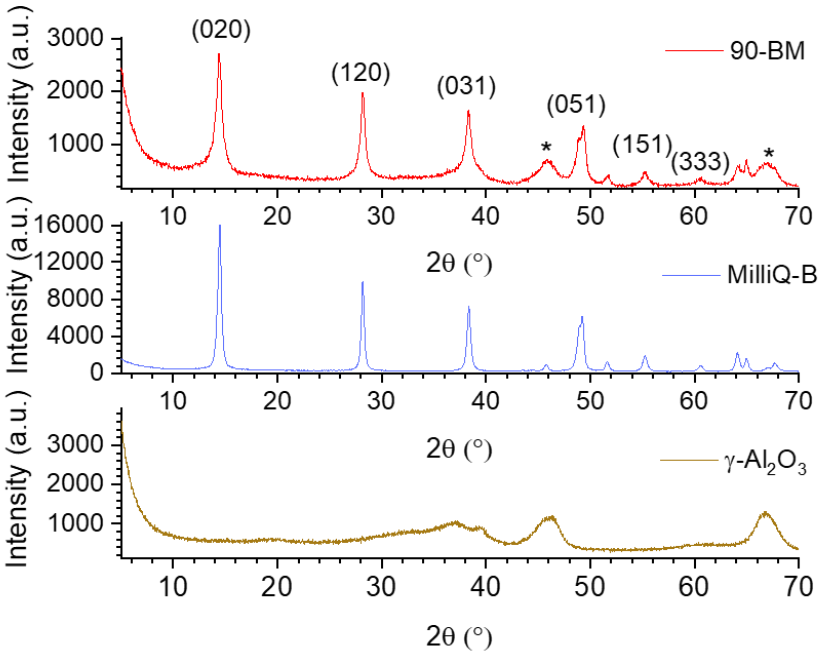

Figure S1: (A.) PXRD patterns of t-BM samples (t = 5, 15, 30, 60, 90 min) between 4° and 24° focusing on the MOF(Al) diffraction region. (B.) Comparison of PXRD patterns for γ-Al_2O_3, MilliQ-B and 90-BM samples.

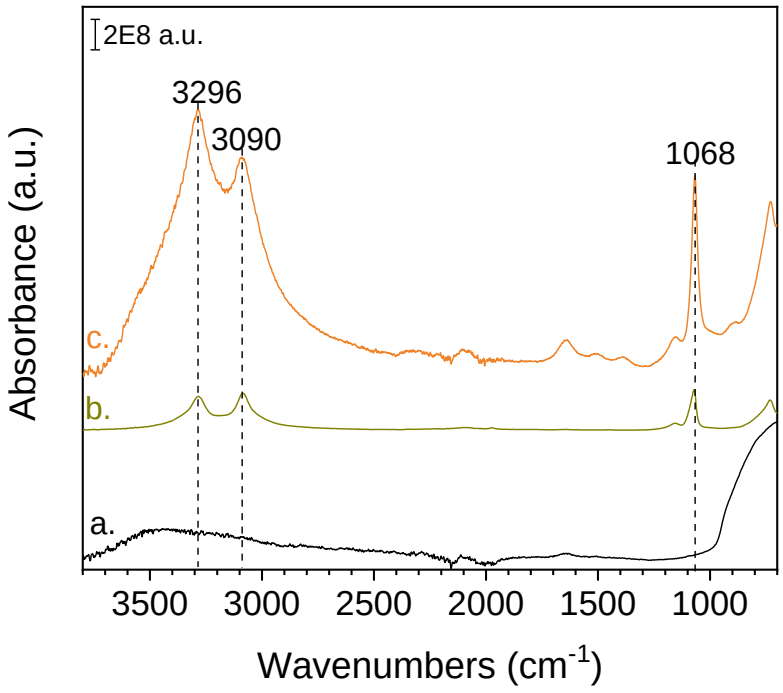

Figure S2: IR-ATR spectra of (a.) calcined boehmite at 500°C for 3h to obtain γ-Al_2O_3. (b.) as obtained γ-Al_2O_3 treated hydrothermally in Milli-Q water under MW-irradiation for 90 min (220°C, 44°C/min, 600 W. (c.) pristine boehmite powder. We note a re-conversion of γ-Al_2O_3 to boehmite after MW-assisted hydrothermal reaction at 220°C due the appearance of hydroxide absorption bands at 3296, 3090 and 1068 cm^{-1}.

Table S1: Average weight percent concentrations of C, N, O and Al atoms determined by EDX for t-BM samples (t = 5, 15, 30, 60, 90 min) prepared by MW-assisted hydrothermal reaction at 220°C (44°C/min, 600W).

Reaction time (min)	**[C]** wt%	**[N]** wt%	**[O]** wt%	**[Al]** wt%
5	35.8 ± 5.6	1.5 ±0.7	33.3 ± 6.4	29.3 ± 6.2
15	40.0 ± 8.0	1.8 ± 0.4	34.0 ±2.9	24.4 ± 6.1
30	34.5 ± 9.4	0.8 ± 0.4	38.0 ± 5.7	26.6 ± 4.3
60	32.6 ± 9.9	1.0 ± 0.4	37.6 ± 3.9	28.8 ± 6.4
90	24.3 ± 2.0	0.8 ± 0.3	44.8 ± 2.1	30.1 ± 2.8

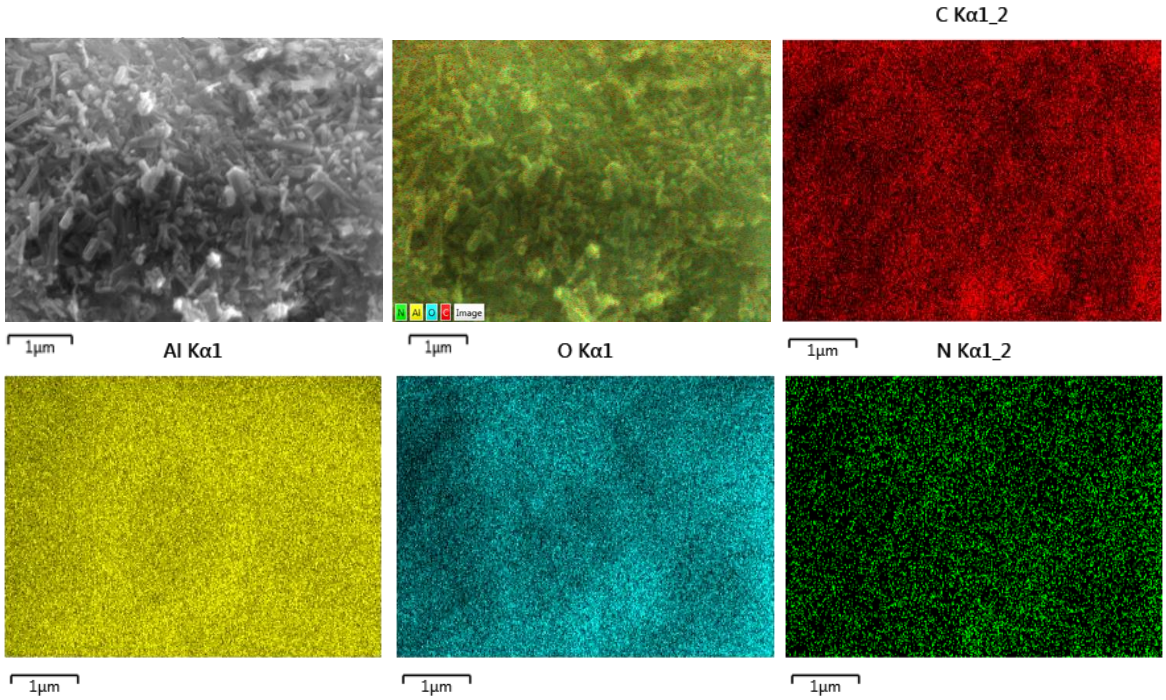

Figure S3: EDX mapping of C, Al, O, and N for the sample 5-BM, showing a homogeneous distribution of atoms over the sample.

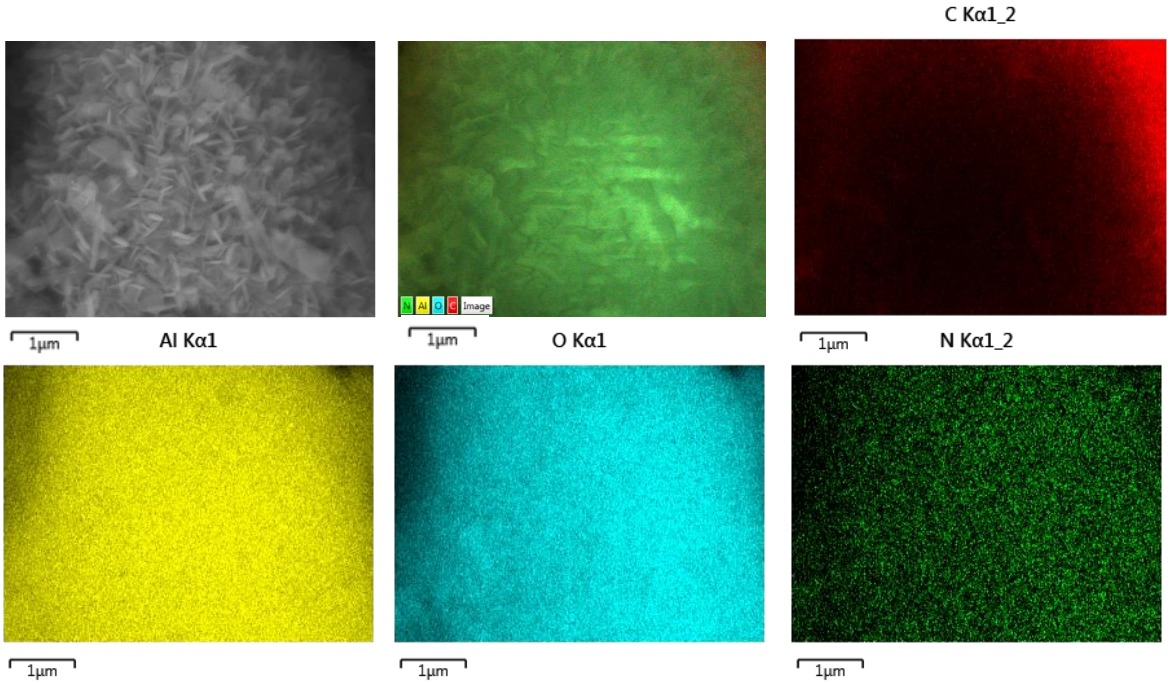

Figure S4: EDX mapping of C, Al, O, and N for the sample 90-BM, showing a homogeneous distribution of Al and O atoms over the sample while C is barely detected. The mapping of N should not be taken into account since its concentration is close to the detection limit.

Table S2: Color evolution of t-BM samples and reaction medium containing only NH2-H2BDC and H_2O in the absence of alumina substrate, between 5 and 90 min at 220°C under MW irradiation (44°C/min, 600 W).

Reaction time (min)	**0**	**5**	**15**	**30**	**60**	**90**
Color of reaction medium in absence of alumina						
Samples' color						

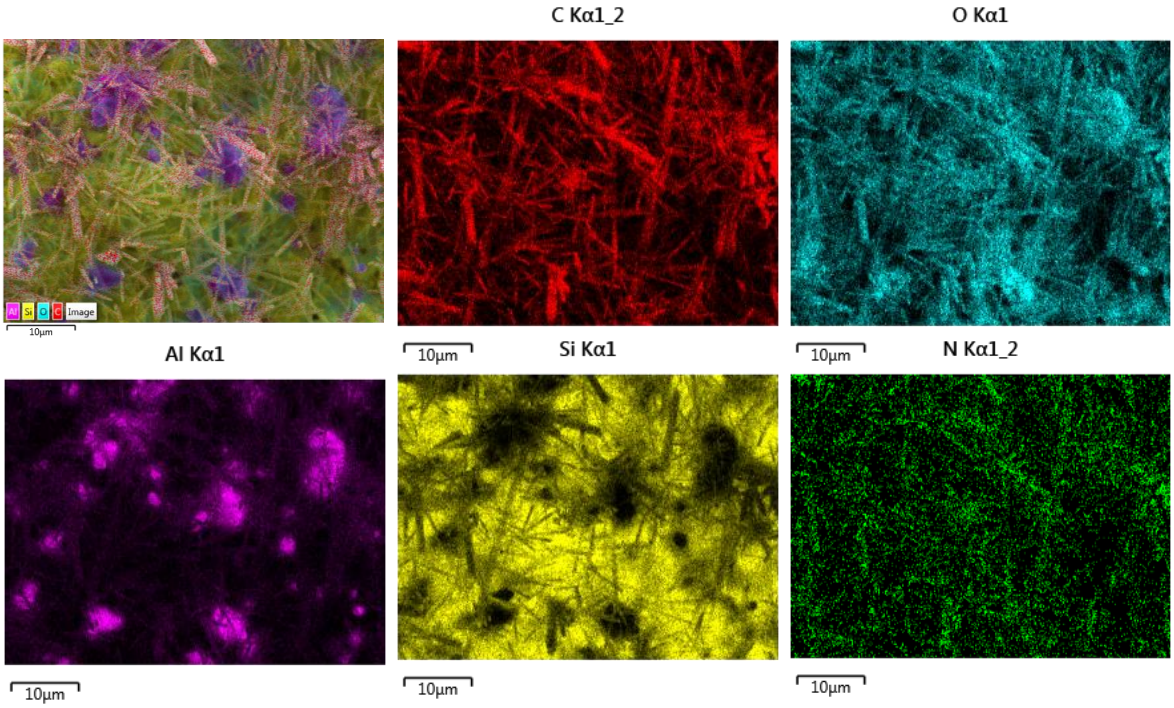

Figure S5: EDX mapping of MOF(Al) crystals grown directly on SiC foams by MW-assisted conversion of ALD-alumina in the presence NH2-H2BDC at 220°C for 90 min (44°C/min, 600W), showing the distributions of C, O, Al and Si atoms.

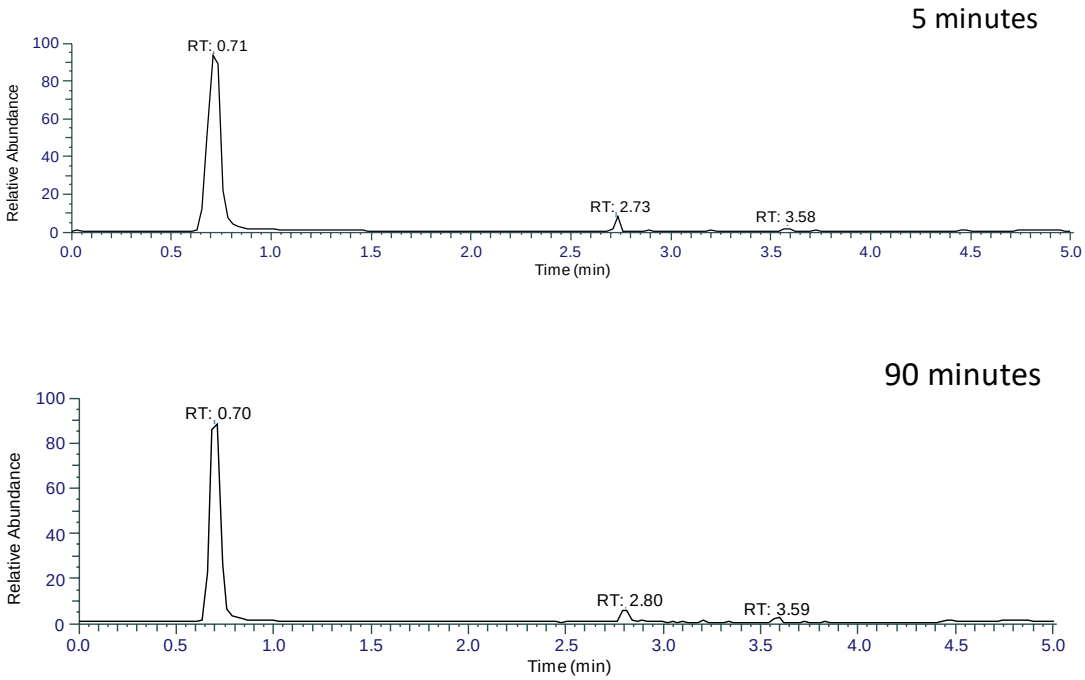

Figure S6: ESI-FTMS chromatograms of the reaction medium (water + NH2-H2BDC) analyzed after 5 and 90 min of reaction (at 220°C, 44°C/min, 600W) in the absence of alumina substrate.

Table S3: Results of FTMS-ESI analysis of the reaction medium (water + NH2-H2BDC) after 5 and 90 min of reaction (220°C, 44°C/min, 600W) in the absence alumina substrate.

Reaction time (min)	Retention time (min)	Empirical formula
5	0.70	$C_7H_8O_2N$
	2.80	$C_{14}H_{13}O_3N_2$
	3.59	$C_{10}H_{11}O_2$
90	0.70	$C_7H_8O_2N$
	2.80	$C_8H_6O_3N$
	3.59	$C_{10}H_{11}O_2$

$C_7H_8O_2N$ corresponds to the decarboxylated form ($-CO_2$) of NH2-H2BDC. According to the results of ^{13}C NMR and ESI-FTMS, $C_{14}H_{13}O_3N_2$ and $C_8H_6O_3N$ are organic polymerized aromatic compounds. The contribution of the benzene ring is always observable on the NMR spectrum and the degree of unsaturation (D = 2C+2+N−X−H2/2) is 9 and 6 respectively implying the presence of several rings and Csp^2.

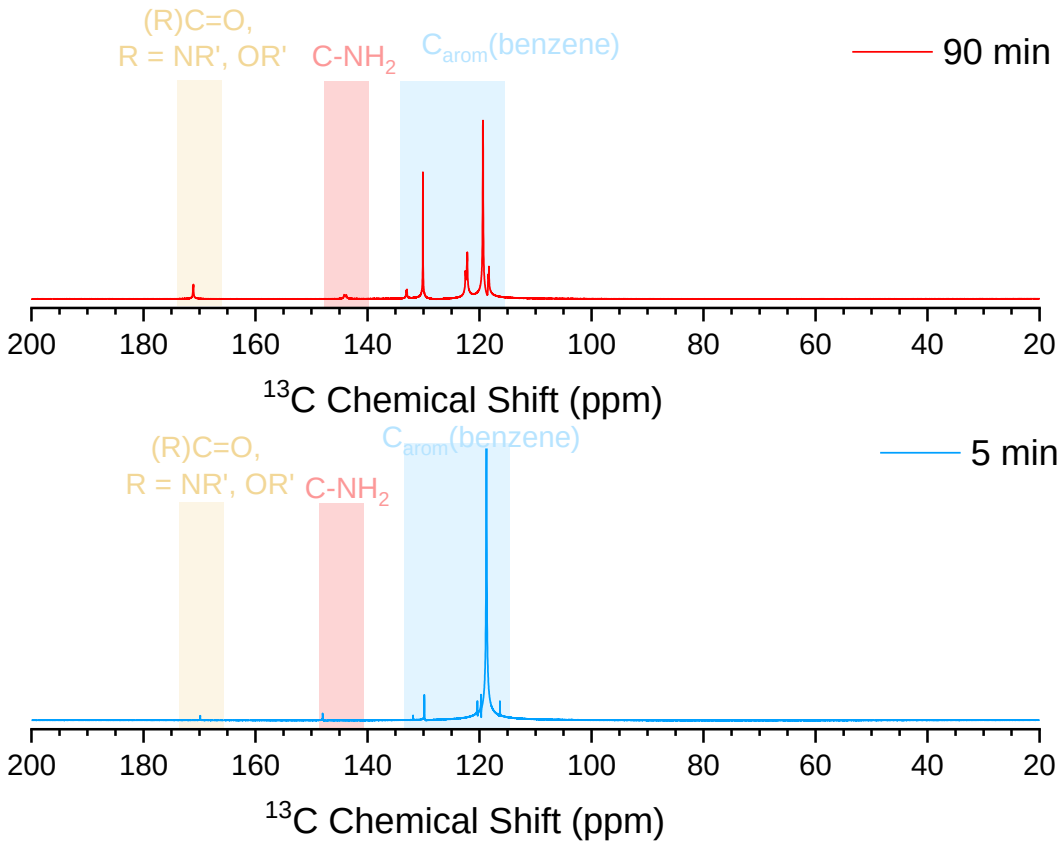

Figure S7: NMR^{13}C (500 MHz, CD_3Cl_3) spectra of the reaction medium (water + NH2-H2BDC), in the absence of alumina substrate after 5 and 90 min of reaction at 220°C (44°C/min, 600W).

Since the MW-assisted hydrothermal reaction of NH_2-H_2BDC in water generates a mixture of organic compounds as demonstrated by ESI-FTMS analysis, and their exact molecular structure is unclear, the analysis of NMR spectra is complex. ^1H NMR analysis was not conducted because the solvent used

during the reaction is water. Hence, ^{13}C NMR was preferred, which allowed us to deduce several interesting information about the organic compounds formed after a reaction time of 5 and 90 min:

-First, on the ^{13}C NMR spectra, no chemical shift is observed above 180 ppm and below 100 ppm, which means that aldehyde, ketones and alkali groups are not present.

-Second, we observe a chemical shift at 169 ppm after 5 min reaction, which shifts to 171 ppm after 90 min. Thus, the chemical environment of the ester carbon or amide carbon has changed. We also note a comparable shift for the carbon linked to an amine shifting from 148 ppm after 5 min reaction to 143 ppm after 90 min. Moreover, we also observe the appearance of a chemical shift at 122 ppm after 90 min reaction. Potentially this peak could be related to an aromatic carbon linked to the carbon atom of an amide or an ester.

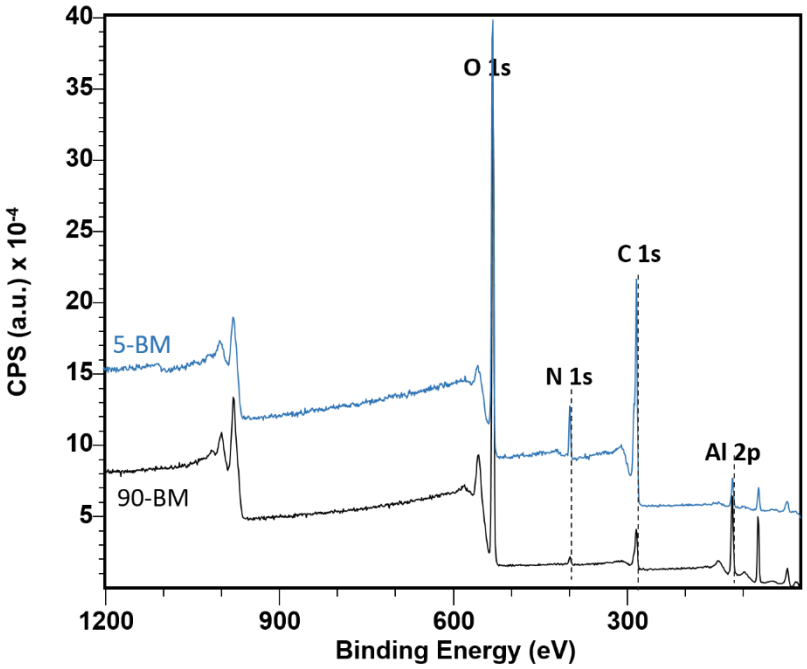

Figure S8: XPS spectra of the 5-BM (blue) and 90-BM (black) samples.

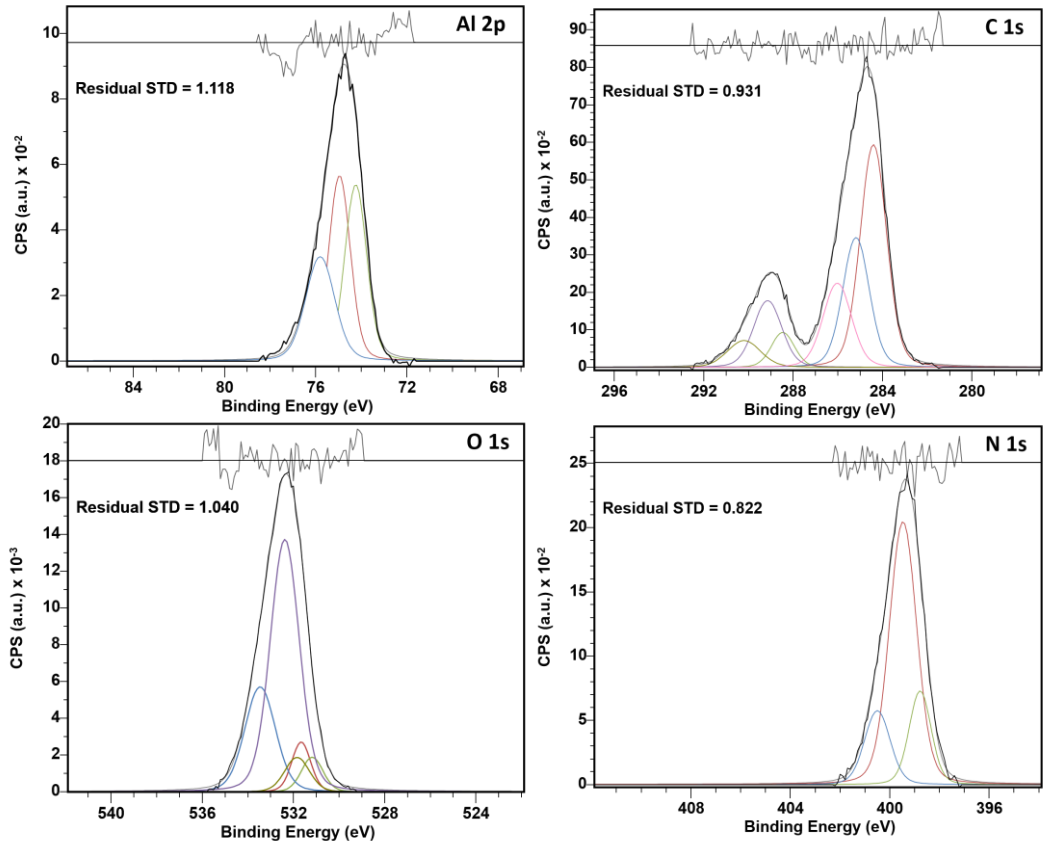

Figure S9: XPS deconvolution spectra of Al, C, N and O bands for the 5-BM sample.

Table S4: XPS deconvolution results for 5-BM sample, summarizing peak attribution, binding energy (BE) and atomic concentration.

Peak designation	Attribution	BE (eV)	FWHM	Concentration (%mol.)	Concentration (%at.)
Al 2p	Al_2O_3	74.2	1.1	35.4	7.4
	Al-OH	74.9	1.1	36.8	
	AlOOH	75.8	1.5	27.8	
N 1s	Amine	398.8	1.0	18.4	6.3
	Amide	399.5	1.3	64.6	
	N^+	400.5	1.2	16.9	
O 1s	AlOOH	531.2	1.1	-	34.5
	Al_2O_3	531.7	1.0		
	Al-OH	531.8	1.2		
	O=C	532.4	1.5		
	O-C/O-H	533.5	1.6		
C 1s	C=C	284.4	1.4	-	51.8
	$C\text{-}COO^-$	285.2	1.4		
	C-O/C-N	286.0	1.5		
	N-C=O	288.5	1.2		
	O-C=O	289.1	1.5		
	Satelite $\pi \rightarrow \pi^*$	290.2	2.1		

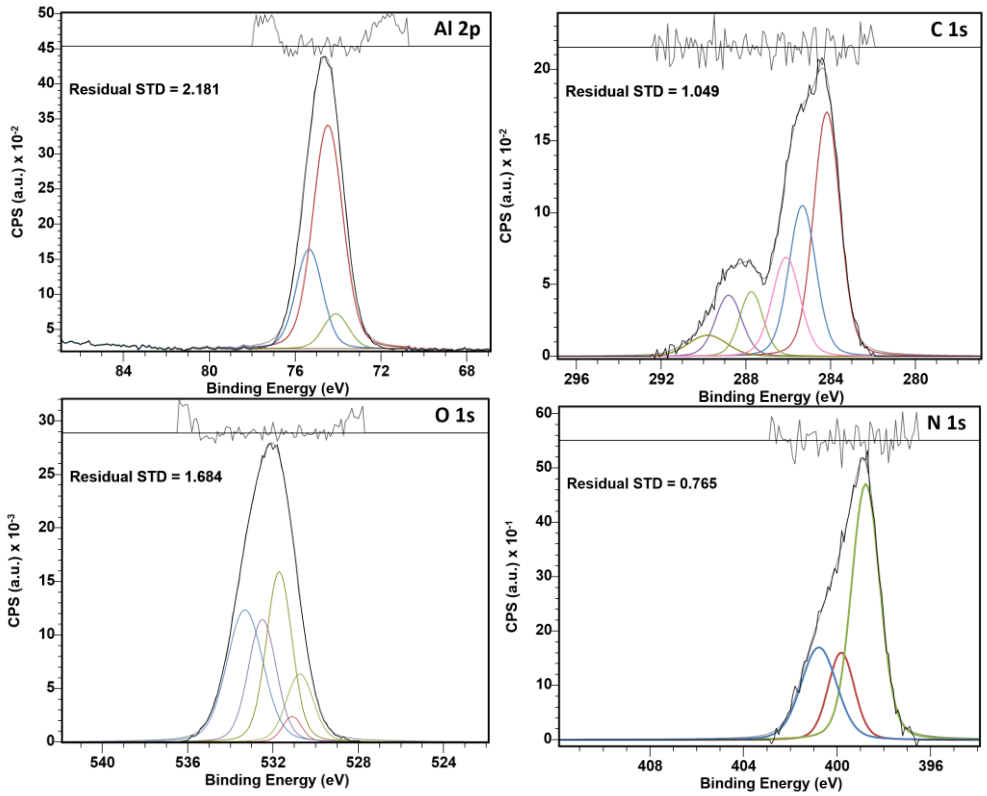

Figure S10: XPS deconvolution spectra of Al, C, N and O bands for the 90-BM sample.

Table S5: XPS deconvolution results for 90-BM sample, summarizing peak attribution, binding energy (BE) and atomic concentration.

Peak designation	Attribution	BE (eV)	FWHM	Concentration (%mol.)	Concentration (%at.)
Al 2p	Al_2O_3	74.1	1.4	8.7	27.1
	Al-OH	74.5	1.6	65.5	
	AlOOH	75.3	1.4	25.8	
N 1s	Amine	398.8	1.4	56.6	1.5
	Amide	399.8	1.3	17.8	
	N^+	400.8	1.8	25.6	
O 1s	AlOOH	530.7	1.5	-	57.5
	Al_2O_3	531.1	1.2		
	Al-OH	531.7	1.4		
	O=C	532.5	1.5		
	O-C/O-H	533.3	2.0		
C 1s	C=C	284.2	1.5	-	13.8
	$C\text{-}COO^-$	285.3	1.5		
	C-O/C-N	286.1	1.5		
	N-C=O	287.8	1.3		
	O-C=O	288.8	1.5		
	Satellite π → π*	289.8	2.1		